Adsorption

DOI: 10.1002/anie.201205258

An MoS_x Structure with High Affinity for Adsorbate Interaction**

*Dezheng Sun, Wenhao Lu, Duy Le, Quan Ma, Maral Aminpour, Marisol Alcántara Ortigoza, Sarah Bobek, John Mann, Jonathan Wyrick, Talat S. Rahman, and Ludwig Bartels**

MoS_2 is an intriguing material: although its basal plane is quite inert, it is the key catalyst for petrochemical hydrodesulfurization (and hydrodenitrogenation) processes. Dow/Union Carbide developed an MoS_2-based catalyst[1] for the formation of higher alcohols from syngas, an application which is gaining increased importance with the emergence of biofuels. In these applications, MoS_2 is used as a fine powder; cobalt or nickel (or mixtures thereof) activate the powder through incorporation into edges of the MoS_2[2] structures. Further promotion is achieved by alkali doping with carbon typically serving as the support.[3] Quite recently, MoS_2 has attracted increasing interest as an exfoliatable monolayer material for (opto-)electronic applications,[4] and as a surface material for electrochemical reactions,[5] among other applications.

Several studies have succeeded in growing MoS_2 on various substrates and have shown that its catalytic activity may be ascribed to a metallic electronic state at the brim of MoS_2 triangular clusters, which can be readily identified in scanning tunneling microscopy (STM).[6–8] We have recently developed a technique for growing MoS_2—by evaporating molybdenum on a sulfur-preloaded Cu(111) surface—that leads to epitaxial MoS_2 islands of sizes ranging from approximately 1 to 100 nm and for which we have confirmed the presence of the brim state.[9] Herein, we demonstrate that another novel MoS_x structure, reproducibly formed in the same fashion as in the growth of MoS_2 we recently performed, is stable in the entire temperature range of our experiments (25 K to 650 K) and reverts to its pristine form after exposure to oxygen-containing adsorbates upon annealing. More importantly, this structure interacts far more strongly with these adsorbates than MoS_2. Analysis of STM images and related electronic structure calculations confirm the metallic nature of this monolayer material, which we rationalize below to have the composition Mo_2S_3.

We chose anthraquinone (AQ) as test adsorbate, because it is large and rigid enough that we can directly image its adsorption geometry, from which we can derive insight into the interaction of the surface with the adsorbate.

The sample preparation described in the Supporting Information gives two thermally stable MoS_x patterns (Figure 1a). The patches formed by both patterns are capable of extending across substrate steps. Regions not covered with an MoS_x patch exhibit the well-known $(\sqrt{7}\times\sqrt{7})$R19° Cu–S overlayer (abbreviated $\sqrt{7}$ in the following) that forms on Cu(111). Although this Cu–S overlayer has been studied extensively both experimentally and through calculations, its atomic-level setup remains in debate.[10–12] Our DFT calculations of the vibrational spectra at the surface Brillouin zone center (Γ) for some of the proposed hexagonal $\sqrt{7}$ sulfur terminations of Cu(111) show both the structure reported by Domange and Oudar[12] and the Cu_4-based structure studied by Foss[11] to be dynamically stable. Although the phonon densities of states at Γ show structure-distinctive frequencies, the differences between the two spectra are too subtle to determine an energetic difference. In the following, we assume that the structure proposed by Domange and Oudar is correct (Figure 1c), because experimental and theoretical work supports it so far.

MoS_2 is one of the MoS_x patterns we observed (Figure 1b). All MoS_2 films and islands were found to align with the crystallographic axes of the substrate, and they appear in STM with a characteristic Moiré pattern caused by the epitaxial growth of (4×4) unit cells of MoS_2 on (5×5) atoms of the Cu(111) substrate (Figure 1b).[9] These islands also feature the electronic brim state, described in detail by Besenbacher and co-workers for MoS_2 synthesis on gold,[8,13] to which the catalytic activity of MoS_2 has been attributed.

The other MoS_x pattern corresponds to well-ordered islands that have a unit cell with $\sqrt{7}$-long sides (similar to the hexagonal $\sqrt{7}$ structure), but at angles of 82° and 98°—or $\begin{bmatrix} 2 & 1 \\ -2 & 3 \end{bmatrix}$ in vector notation. The pattern provides the closest approximation to a square unit cell achievable with short unit vectors on an fcc(111) surface. Although a number of molybdenum–sulfur structures have been described (including bulk Mo_2S_3),[7,14] to our knowledge, there is no prior reference to this nearly square structure. We found up to 20% of the sample surface covered by this structure. After a thorough computational screening of about 50 possible MoS_x structures on Cu(111), targeted to find the lowest-energy structure and the one whose calculated STM image most resembled the

[*] Dr. D. Sun, M. Sc. W. Lu, M. Sc. Q. Ma, S. Bobek, M. Sc. J. Mann, M. Sc. J. Wyrick, Dr. L. Bartels
Pierce Hall, University of California
Riverside, CA 92521 (USA)
E-mail: bartels@ucr.edu
Dr. D. Sun
Department of Physics, Columbia University
New York, NY 10027 (USA)
Dr. D. Le, M. Sc. M. Aminpour, Dr. M. Alcántara Ortigoza, Dr. T. S. Rahman
Department of Physics, University of Central Florida
Orlando, FL 32816 (USA)

[**] We gratefully acknowledge support from the US Department of Energy (Columbia, UCF, UCR: DE-FG02-07ER15842) for simulation and analysis of the reactive properties of MoS_x films, and the US National Science Foundation (UCR, Columbia U.: DMR 1106210) for novel methods for the growth of MoS_2 and related films.

Supporting information for this article is available on the WWW under http://dx.doi.org/10.1002/anie.201205258.

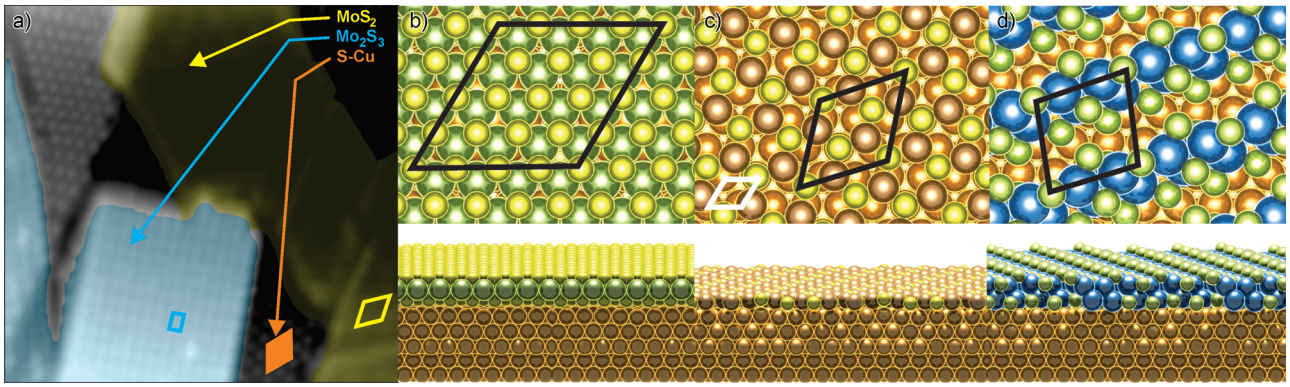

Figure 1. a) STM image of MoS_x structures. Models of b) MoS_2/Cu(111), c) $\sqrt{7}$ sulfur-terminated copper (S–Cu), and d) Mo_2S_3 structure at the focus of this manuscript. Imaging parameters: bias: −0.93 V, current: 0.21 nA, scale bar: 5 nm. Models: Cu = brown, S = yellow, Mo = green/blue.

observed one, we found good correspondence of these nearly square patches with the properties of an Mo_2S_3 layer (Figure 1 d). In the following, we will describe some observations (experimental and computational) that support this structural model and will highlight its chemical properties. The geometry that we found to best match our experimental observations while at the same time being structurally stable on Cu(111) contains four molybdenum atoms and six sulfur atoms per $\begin{bmatrix} 2 & 1 \\ -2 & 3 \end{bmatrix}$ unit cell (i.e., Mo_2S_3); it arranges the molybdenum atoms in approximately an upright square which is stabilized along its sides by the sulfur atoms (Figure 1 d).

As we were not aware of any precedence for this MoS_x structure, establishing its unit cell composition and internal geometry was not trivial: diffraction was no help here, as both the $\sqrt{7}$ sulfur termination of copper and the novel structure are set up from $\sqrt{7}$ unit vectors and coexist on the surface. We validated the presence of molybdenum in this structure in preparations identical to the one mentioned in the Supporting Information, yet leaving out the deposition of molybdenum resulted in the formation of exclusively the $\sqrt{7}$ sulfur termination of copper. We note that surrounding the MoS_2 islands we frequently found sulfur depletion of the $\sqrt{7}$ structure.[9] This is, however, not the case around the Mo_2S_3 islands, in agreement with their lower sulfur surface density (Figure 1 d).

Figure 2 a shows an STM image in which all three structures are present adjacent to each other in a single scan line: on the left is an MoS_2 island, in the center the $\sqrt{7}$ sulfur-terminated copper, and on the right an Mo_2S_3 patch. Also visible is some depletion of the $(\sqrt{7} \times \sqrt{7})R19°$ sulfur atoms directly adjacent to the MoS_2 layer. The top portion of that image is DFT-derived simulated topography as an isosurface of energy-integrated (from −1.0 to 0 eV) local density of states of 10^{-4} e Å^3 convoluted with a tip radius of 2.4 Å. While each structure was calculated separately (hence not showing any edge effects), the relative heights of the structures were referenced to the bottommost of the five substrate layers in the DFT simulation, thus permitting no adjustable parameter in the height profile between simulation and experiments (both image portions use the same grayscale). Not only are the relative heights reproduced well, but even subtleties, such

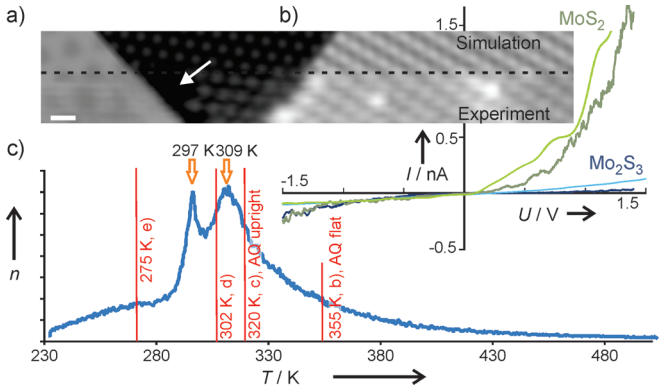

Figure 2. a) STM image (below the dashed line) and simulation (above the dashed line) of a sample with MoS_2, S–Cu, and Mo_2S_3 (left to right) in a single scan line. Also shown is depletion of the S–Cu surface directly adjacent to the MoS_2 island (white arrow). Scale bar: 1 nm; tip height stabilized at 0.15 nA at −1.04 V bias. b) I/V spectra obtained on MoS_2 and Mo_2S_3 (darker lines), and simulated I/V curves (lighter lines); same imaging conditions as above. c) Thermal desorption spectroscopy of AQ fragments (masses: 50, 77) shows two signals corresponding to AQ adsorbed on MoS_2 and $\sqrt{7}$ S–Cu, and a high-temperature shoulder for desorption from the two configurations on Mo_2S_3. The red labels indicate the STM images that can be obtained after annealing to these temperatures by referring to the panels of Figure 3.

as the amplitude and alignment of the Moiré pattern on the MoS_2, are represented convincingly.

Scanning tunneling spectroscopy performed on MoS_2 and Mo_2S_3 layers resulted in fundamentally different spectra (Figure 2 b): on MoS_2 we found comparatively little variation of the tunneling current at negative sample bias, but large variation at positive bias, indicating the MoS_2 conduction band edge. In contrast, on Mo_2S_3 we found little variation of the current at either polarity, attesting to the absence of band edges near the Fermi level, in agreement with DFT simulations, which were averaged over the Mo_2S_3 unit cell area. The Supporting Information contain dI/dV spectra, which indicate a bandgap of approximately 1.4 eV for MoS_2, in good agreement with recent studies on MoS_2 devices with metallic contacts.[15] The comparatively high abundance of the Mo_2S_3

layer posed the question of its relevance for surface reactions and surface catalytic activity. To elucidate the capability of this structure to interact with adsorbates, we exposed it to a molecular species, anthraquinone (Figure 3), which was chosen for ease of imaging in STM.

Figure 3 shows images obtained on the same surface at increasing exposure of AQ from panels b to e. Exposure proceeded at near-liquid-nitrogen temperature followed by annealing just below room temperature. Contrary to our expectation of preferential adsorption of AQ at the brim states of MoS_2, we found AQ to adsorb exclusively at the Mo_2S_3 structure (Figure 3a). Initially, AQ forms molecular rows at intermolecular distances of $\sqrt{7}$, quite similar to AQ rows on Cu(111) (and on the $\sqrt{7}$ structure, see below), for which we found the presence of non-negligible intermolecular hydrogen bonds.[16] On further increasing the dosage of AQ, we observed an increase in the coverage exclusively on the Mo_2S_3 structure until a dense layer of AQ molecules, adsorbed parallel to the substrate (Figure 3b), is formed. Increasing the coverage further leads to a denser packing of the AQ layer on the Mo_2S_3 structure (Figure 3c), and the AQ molecules continue to avoid the sulfur-terminated substrate, as well as the MoS_2 islands, with their supposedly reactive brim states.

We performed DFT simulations of the two adsorption configurations of AQ on Mo_2S_3 that we observed experimentally: in agreement with the experimental observations, minimization of the adsorption configuration results in registry, periodicity, and alignment (Figure 4). In the planar configuration, both AQ carbonyl groups are in close proximity to the top molybdenum atoms of the Mo_2S_3 structure (Figure 4a); in the upright configuration, the bottom carbonyl group adsorbs on one of the molybdenum centers, resulting in a slight rearrangement of the Mo_2S_3 structure (Figure 4c). We find the binding energy to be 3.36 eV and 1.92 eV in the planar and upright configuration, respectively.

Once all Mo_2S_3 is covered, AQ populates the sulfur-terminated copper surface (Figure 3d), including the areas near the MoS_2 and Mo_2S_3 island edges. Here, AQ preferentially forms close molecular rows, optimizing intermolecular hydrogen bonding, as discussed in previous publications.[16] Because of the geometry and size of the $\sqrt{7}$ S–Cu structure and its incommensurability with AQ, molecular rows in adjacent surface unit cells do not generate a closely packed AQ

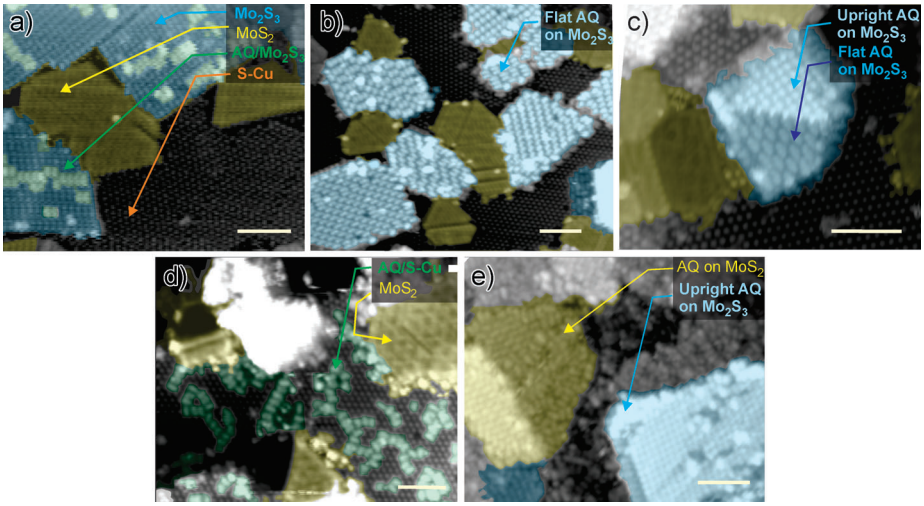

Figure 3. STM images of increasing AQ coverages on the different surface structures (panels b–e correspond to 0.1, 0.3, 1.5, and 2.7 Langmuir, respectively). Initially, AQ forms a) rows on Mo_2S_3, followed by a complete coverage of Mo_2S_3 with first b) horizontally and next c) uprightly adsorbed molecules. Only subsequently do d) molecular rows form on the $\sqrt{7}$ structure until finally e) MoS_2 is covered. The scale bars are 5 nm. Imaging parameters: a) bias: −4.33 V, 0.24 nA b) bias: −1.66 V, 0.17 nA; c) bias: −0.83 V, current 0.34 nA; d) bias: −0.92 V, current 0.11 nA; e) bias −2.75 V, current: 0.13 nA.

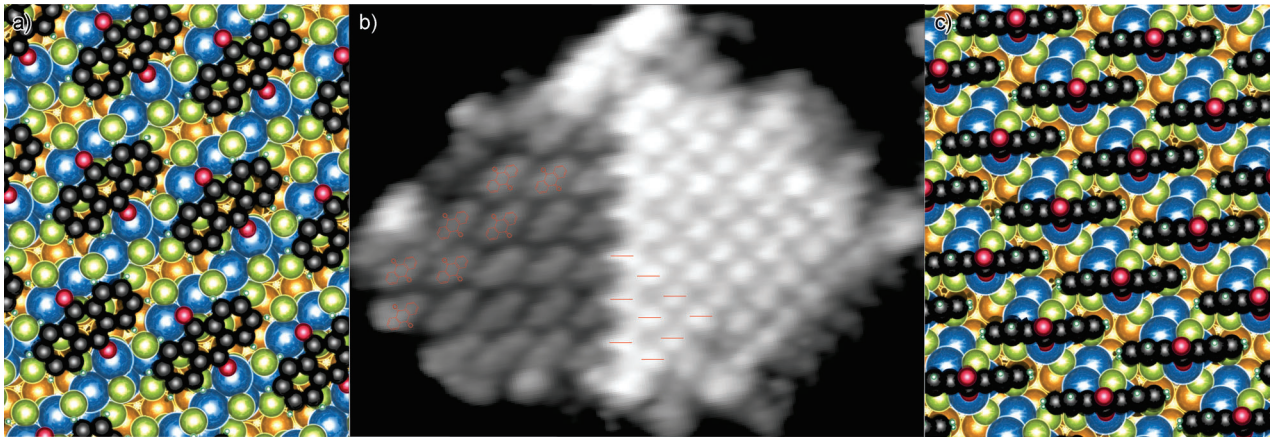

Figure 4. a, c) DFT-optimized adsorption geometry of AQ on Mo_2S_3 in horizontal and vertical adsorption configuration, respectively, and b) STM image (magnification of the island in Figure 3c) showing the coexistence and relative orientation of the molecules. Imaging parameters: bias = −0.83 V, current = 0.34 nA, scale bar: 5 nm.

layer (in contrast to what occurs on Mo_2S_3), and we observed the absence of long-range 2D order on this surface. The Supporting Information contain the calculated adsorption structure and a higher-magnified STM image. The calculated adsorption energy of AQ on the sulfur-terminated copper surface is 1.47 eV, lower than that on the Mo_2S_3 structure, even in the upright configuration.

AQ molecules only populate the MoS_2 islands and their brim areas after the sulfur-terminated copper surface is covered. Here, AQ preferentially forms an array of molecular rows, which are in anti-phase with adjacent rows, though occasionally in-phase lateral stacking of rows is also observed. The spacing of AQ molecules (at 6.75 Å center to center) is very tight, thus enabling intermolecular hydrogen bonding, as discussed previously.[16]

The electronic and optical properties of MoS_2 in the presence of a substrate have already been analyzed by ab initio calculations.[17] Because the periodicity of the AQ layer on MoS_2 is incommensurate with the Moiré superstructure of the (4×4) MoS_2 layer, we calculated the adsorption energy of 1.32 eV by modeling an isolated molecule on a MoS_2/Cu slab (1.20 eV) and adding to that the lateral AQ–AQ interactions calculated on a MoS_2 monolayer (0.12 eV). The hierarchy of the DFT adsorption energies is thus in agreement with the relative preference for AQ adsorption on the three different surface structures that we report here. The Supporting Information contains the calculated adsorption structure.

Thermal desorption spectroscopy of AQ gives the trace shown in Figure 2c. Through a sequence of partial annealing and STM imaging, we correlated its features to the structures shown in the referenced panels of Figure 3: heating to 275 K results in a complete coverage of the surface (Figure 3e); the signal at 297 K corresponds to AQ adsorbed on MoS_2/Cu(111), imaging after heating to 302 K shows AQ only on the sulfur-terminated copper and on Mo_2S_3 (Figure 3d); the signal at 309 K corresponds to AQ/S–Cu, and its broad high-temperature tail to the two AQ configurations on Mo_2S_3; imaging at 320 K and 355 K shows AQ exclusively upright and flat (Figures 3c and b), respectively. The absence of a sharp signal and the proximity of the signals of the latter configurations show how these structures may have been overlooked in previous spectroscopic studies. Increase of the substrate temperature above 500 K results in a clean surface with the three surface morphologies shown in Figures 1 and 2. The sequence of desorption temperatures are in agreement with our theoretical modeling of binding energies; the calculated energy values for all structures are higher than what one would expect from the desorption experiment, thus attesting to the challenges of modeling van der Waals interaction in unit cells of this size and complexity.

The finding of a thermally stable molybdenum–sulfur structure that has higher affinity for adsorbate interaction than the much discussed MoS_2 brims is exciting and suggestive of its relevance to existing catalytic applications, or its utility as an inverse catalyst,[18] yet reactor studies will be necessary to confirm its relevance conclusively. We also attempted to adsorb CO on the MoS_x structures, but could not resolve its image on the surface, probably because it was moving too rapidly at a sample temperature of approximately 25 K (CO starts diffusing on Cu(111) at around 40 K and the passivated surfaces investigated here offer CO interactions that are weaker than those of metallic copper, as shown in our calculations).[19]

In conclusion, we found a novel MoS_x surface structure on copper, which we propose to have the composition Mo_2S_3, whose ability to interact and activate adsorbates far exceeds that of MoS_2 while proving to be of similar thermal stability and also recoverable after adsorption through annealing. Some catalyst compositions of MoS_x for the formation of products from syngas contain copper;[1] thus, our finding of a high affinity MoS_x composition specifically on copper may point toward an alternative origin of the actual working of such a catalyst, if further corroborated by studies at high pressure.

Received: July 4, 2012
Published online: September 11, 2012

Keywords: adsorption · anthraquinone · molybdenum · monolayers · MoS_2

[1] V. R. Surisetty, A. K. Dalai, J. Kozinski, *Appl. Catal. A* **2011**, *404*, 1–11.
[2] a) C. R. F. Lund, *Ind. Eng. Chem. Res.* **1996**, *35*, 3067–3073; b) G. Z. Bian, Y. L. Fu, Y. S. Ma, *Catal. Today* **1999**, *51*, 187–193; c) S. Zaman, K. J. Smith, *Catal. Rev.* **2012**, *54*, 41–132.
[3] a) X. G. Li, L. J. Feng, Z. Y. Liu, B. Zhong, D. B. Dadyburjor, E. L. Kugler, *Ind. Eng. Chem. Res.* **1998**, *37*, 3853–3863; b) L. J. Feng, X. G. Li, D. B. Dadyburjor, E. L. Kugler, *J. Catal.* **2000**, *190*, 1–13; c) X. G. Li, L. J. Feng, L. J. Zhang, D. B. Dadyburjor, E. L. Kugler, *Molecules* **2003**, *8*, 13–30.
[4] a) K. F. Mak, C. Lee, J. Hone, J. Shan, T. F. Heinz, *Phys. Rev. Lett.* **2010**, *105*, 136805; b) A. Splendiani, L. Sun, Y. Zhang, T. Li, J. Kim, C.-Y. Chim, G. Galli, F. Wang, *Nano Lett.* **2010**, *10*, 1271–1275.
[5] Z. Chen, J. Kibsgaard, T. F. Jaramillo, *Proc. SPIE*, *Vol. 7770*, **2010**, p. 77700K.
[6] a) S. Helveg, J. Lauritsen, E. Laegsgaard, I. Stensgaard, J. Norskov, B. Clausen, H. Topsoe, F. Besenbacher, *Phys. Rev. Lett.* **2000**, *84*, 951–954; b) J. Kibsgaard, J. V. Lauritsen, E. Lagsgaard, B. S. Clausen, H. Topsoe, F. Besenbacher, *J. Am. Chem. Soc.* **2006**, *128*, 13950–13958; c) J. V. Lauritsen, J. Kibsgaard, S. Helveg, H. Topsoe, B. S. Clausen, E. Laegsgaard, F. Besenbacher, *Nat. Nanotechnol.* **2007**, *2*, 53–58; d) Y.-H. Lee, X.-Q. Zhang, W. Zhang, M.-T. Chang, C.-T. Lin, K.-D. Chang, Y.-C. Yu, J. T.-W. Wang, C.-S. Chang, L.-J. Li, T.-W. Lin, *Adv. Mater.* **2012**, *24*, 2320–2325; e) K.-K. Liu, W. Zhang, Y.-H. Lee, Y.-C. Lin, M.-T. Chang, C.-Y. Su, C.-S. Chang, H. Li, Y. Shi, H. Zhang, C.-S. Lai, L.-J. Li, *Nano Lett.* **2012**, *12*, 1538–1544; f) C. Kisielowski, Q. M. Ramasse, L. P. Hansen, M. Brorson, A. Carlsson, A. M. Molenbroek, H. Topsoe, S. Helveg, *Angew. Chem.* **2010**, *122*, 2768–2770; *Angew. Chem. Int. Ed.* **2010**, *49*, 2708–2710; g) L. P. Hansen, Q. M. Ramasse, C. Kisielowski, M. Brorson, E. Johnson, H. Topsoe, S. Helveg, *Angew. Chem.* **2011**, *123*, 10335–10338; *Angew. Chem. Int. Ed.* **2011**, *50*, 10153–10156.
[7] J. Kibsgaard, A. Tuxen, M. Levisen, E. Laegsgaard, S. Gemming, G. Seifert, J. V. Lauritsen, F. Besenbacher, *Nano Lett.* **2008**, *8*, 3928–3931.
[8] M. Bollinger, J. Lauritsen, K. Jacobsen, J. Norskov, S. Helveg, F. Besenbacher, *Phys. Rev. Lett.* **2001**, *87*, 196803.

[9] D. Kim, D. Sun, W. Lu, Z. Cheng, Y. Zhu, D. Le, T. S. Rahman, L. Bartels, *Langmuir* **2011**, *27*, 11650 – 11653.
[10] a) D. R. Alfonso, *J. Phys. Chem. C* **2011**, *115*, 17077 – 17091; b) M. Saidy, K. A. R. Mitchell, *Surf. Sci.* **1999**, *441*, 425 – 435; c) N. P. Prince, D. L. Seymour, M. J. Ashwin, C. F. McConville, D. P. Woodruff, R. G. Jones, *Surf. Sci.* **1990**, *230*, 13 – 26; d) G. J. Jackson, S. M. Driver, D. P. Woodruff, B. C. C. Cowie, R. G. Jones, *Surf. Sci.* **2000**, *453*, 183 – 190; e) E. Wahlstrom, I. Ekvall, T. Kihlgren, H. Olin, S.-a. Lindgren, L. Wallden, *Phys. Rev. B* **2001**, *64*, 155406; f) K. Motai, T. Hashizume, H. Lu, D. Jeon, T. Sakurai, H. W. Pickering, *Appl. Surf. Sci.* **1993**, *67*, 246 – 251.
[11] M. Foss, R. Feidenhans'l, M. Nielsen, E. Findeisen, T. Buslaps, R. L. Johnson, F. Besenbacher, *Surf. Sci.* **1997**, *388*, 5 – 14.
[12] J. L. Domange, J. Oudar, *Surf. Sci.* **1968**, *11*, 124 – 142.
[13] J. Lauritsen, M. Nyberg, R. Vang, M. Bollinger, B. Clausen, H. Topsoe, K. Jacobsen, E. Laegsgaard, J. Norskov, F. Besenbacher, *Nanotechnology* **2003**, *14*, 385 – 389.
[14] a) J. Zhang, J. M. Soon, K. P. Loh, J. Yin, J. Ding, M. B. Sullivian, P. Wu, *Nano Lett.* **2007**, *7*, 2370 – 2376; b) R. K. Tiwari, J. S. Yang, M. Saeys, C. Joachim, *Surf. Sci.* **2008**, *602*, 2628 – 2633; c) M. L. Tang, D. C. Grauer, B. Lassalle-Kaiser, V. K. Yachandra, L. Amirav, J. R. Long, J. Yano, A. P. Alivisatos, *Angew. Chem.* **2011**, *123*, 10385 – 10389; *Angew. Chem. Int. Ed.* **2011**, *50*, 10203 – 10207.
[15] a) Y. Zhang, J. Ye, Y. Matsuhashi, Y. Iwasa, *Nano Lett.* **2012**, *12*, 1136 – 1140; b) B. Radisavljevic, A. Radenovic, J. Brivio, V. Giacometti, A. Kis, *Nat. Nanotechnol.* **2011**, *6*, 147 – 150.
[16] a) G. Pawin, K. L. Wong, K. Y. Kwon, L. Bartels, *Science* **2006**, *313*, 961 – 962; b) G. Pawin, U. Solanki, K. Y. Kwon, K. L. Wong, X. Lin, T. Jiao, L. Bartels, *J. Am. Chem. Soc.* **2007**, *129*, 12056 – 12057; c) K. Y. Kwon, G. Pawin, K. L. Wong, E. Peters, D. Kim, S. Hong, T. S. Rahman, M. Marsella, L. Bartels, *J. Am. Chem. Soc.* **2009**, *131*, 5540 – 5545.
[17] a) P. Johari, V. B. Shenoy, *ACS Nano* **2011**, *5*, 5903 – 5908; b) D. Le, D. Sun, W. Lu, L. Bartels, T. S. Rahman, *Phys. Rev. B* **2012**, *85*, 075429; c) Q. Yue, J. Kang, Z. Shao, X. Zhang, S. Chang, G. Wang, S. Qin, J. Li, *Phys. Lett. A* **2012**, *376*, 1166 – 1170; d) A. Ramasubramaniam, D. Naveh, E. Towe, *Phys. Rev. B* **2011**, *84*, 205325.
[18] J. A. Rodríguez, J. Hrbek, *Surf. Sci.* **2010**, *604*, 241 – 244.
[19] a) K. L. Wong, B. V. Rao, G. Pawin, E. Ulin-Avila, L. Bartels, *J. Chem. Phys.* **2005**, *123*, 201102; b) A. Heinrich, C. Lutz, J. Gupta, D. Eigler, *Science* **2002**, *298*, 1381 – 1387.

